J|A|C|S COMMUNICATIONS

Published on Web 11/23/2010

Nonaqueous Catalytic Water Oxidation

Zuofeng Chen, Javier J. Concepcion, Hanlin Luo, Jonathan F. Hull, Amit Paul, and Thomas J. Meyer*

Department of Chemistry, University of North Carolina at Chapel Hill, Chapel Hill, North Carolina 27599, United States

Received August 16, 2010; E-mail: tjmeyer@unc.edu

Abstract: The complex $[Ru(Mebimpy)(bpy)(OH_2)]^{2+}$ [Mebimpy = 2,6-bis(1-methylbenzimidazol-2-yl)pyridine; bpy = 2,2′-bipyridine] and its 4,4′-$(PO_3H_2CH_2)_2$bpy derivative on oxide electrodes are water oxidation catalysts in propylene carbonate and 2,2,2-trifluoroethanol (TFE) to which water has been added as a limiting reagent. The rate of water oxidation is greatly enhanced relative to that with water as the solvent and occurs by a pathway that is first-order in H_2O; an additional pathway that is first-order in acetate appears when TFE is used as the solvent.

Significant progress has been made recently in water oxidation catalysis based on single-site catalysts and derivatized electrodes.[1−3] These experiments have been carried out in aqueous solution (typically over limited pH ranges) and driven by chemical or electrochemical oxidation. Water oxidation in Photosystem II occurs at the oxygen-evolving complex (OEC), which is embedded in the hydrophobic thylakoid membrane, with water a limiting reagent.[4] Demonstration of catalytic water oxidation in nonaqueous environments is potentially of considerable interest in adding flexibility to architectures for solar-fuel devices and for gaining insight into the microscopic details of how nonaqueous water oxidation occurs.

We report here sustained electrocatalytic water oxidation in nonaqueous solvents with water as a limiting reagent by the known water oxidation catalyst $Ru(Mebimpy)(bpy)(OH_2)^{2+}$ (**1**) [Mebimpy = 2,6-bis(1-methylbenzimidazol-2-yl)pyridine; bpy = 2,2′-bipyridine] in solution and its derivative $[Ru(Mebimpy)(4,4'-(PO_3H_2CH_2)_2bpy)(OH_2)]^{2+}$ (**1-PO$_3$H$_2$**) [4,4′-$(PO_3H_2CH_2)_2$bpy = 4,4′-bis(methylenephosphonato)-2,2′-bipyridine] on the surfaces of conductive, planar fluoride-doped SnO_2 (FTO) and nanostructured Sn(IV)-doped In_2O_3 (*nano*ITO) films. The mechanism for electrocatalytic water oxidation by the surface-bound catalyst is shown in Scheme 1. Proton-coupled electron transfer (PCET) oxidation of $Ru^{II}-OH_2^{2+}$ to $Ru^{IV}=O^{2+}$ is followed by further one-electron oxidation to $Ru^{V}=O^{3+}$. $Ru^{V}=O^{3+}$ undergoes O-atom transfer to H_2O to give $Ru^{III}-OOH^{2+}$ which, in turn, undergoes further oxidation and release of O_2.[2,3]

Syntheses of catalyst **1** and surface analogue **1-PO$_3$H$_2$** have been reported elsewhere.[2c] *nano*ITO films with a thickness of ∼2.5 μm on ITO (ITO|*nano*ITO) were prepared by a literature procedure.[5] Stable phosphonate surface binding of **1-PO$_3$H$_2$** on FTO or ITO|*nano*ITO occurred following exposure of the slides to 0.2 mM **1-PO$_3$H$_2$** at pH 5 (0.1 M CH_3CO_2H/CH_3CO_2Na) for 12 h. As shown by electrochemical (FTO) or spectrophotometric (*nano*ITO) measurements, the surface loadings were 1.2×10^{-10} mol/cm^2 on FTO[3a] and 1.7×10^{-8} mol/cm^2 (2.5 μm; 6.8×10^{-9} mol cm^{-2} μm^{-1}) on ITO|*nano*ITO.[3b]

Two solvent systems were investigated. One was propylene carbonate (PC) or a mixture of PC and ethylene carbonate (EC,

Scheme 1. Mechanism of Electrocatalytic Water Oxidation in Water by the Single-Site, Surface-Bound Catalyst **1-PO$_3$H$_2$** on Oxide Electrode Surfaces[2,3]

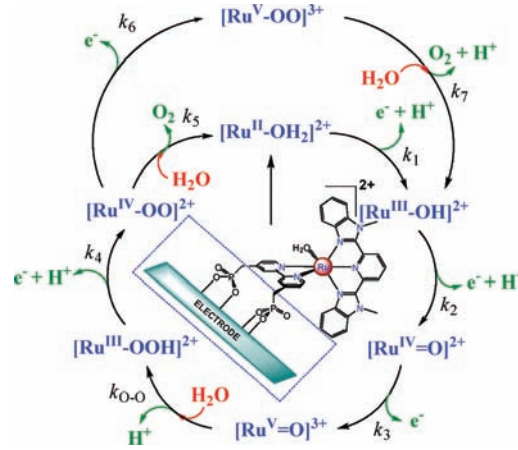

mp = 35 °C). PC is appealing because of its wide potential window with an oxidative limit of >2.0 V (vs NHE), significant water miscibility (∼8% in PC, ∼17% in 1:1 mol/mol PC/EC, and ∼50% in 1:3 mol/mol PC/EC), and weak coordinating ability in comparison with water. The last of these was demonstrated for **1** by the fact that spectrophotometric measurements at $\lambda_{max} = 486$ nm for $Ru(Mebimpy)(bpy)(OH_2)^{2+}$ remained unchanged in PC or PC/EC over a period of 12 h (Figure S1 in the Supporting Information).

We also investigated 2,2,2-trifluoroethanol (TFE), CF_3CH_2OH, as a solvent. It has an oxidative limit of ∼1.85 V (vs NHE). Spectrophotometric measurements provided evidence for solvent coordination with a shift in λ_{max} with time from 486 to 478 nm in neat TFE. Water is favored on a mole-for-mole basis ($K \leq 1 \times 10^{-2}$ for the equilibrium $Ru^{II}-OH_2^{2+} + TFE \rightleftarrows Ru^{II}-TFE^{2+} + H_2O$) in 6% (v/v) water/TFE. In contrast, in 25% (v/v) CH_3CN/H_2O, λ_{max} shifted from 486 nm for the aqua complex to 462 nm for $Ru(Mebimpy)(bpy)(NCCH_3)^{2+}$ with a rate constant (k) of ∼5.9×10^{-4} s^{-1} at room temperature (Figure S2a). Solvent coordination is an important issue in catalysis, since upon loss of the aqua ligand, $Ru^{V}=O^{3+}$ is no longer accessible by PCET oxidation of $Ru^{II}-OH_2^{2+}$ (Figure S2b and Scheme 1).

Cyclic voltammograms (CVs) of 1 mM **1** at a glassy carbon (GC) electrode in 0.1 M $^nBu_4NPF_6$/PC ($^nBu_4N^+$ = tetrabutylammonium cation) with added water are shown in Figure 1a (also see Figures S3 and S4). In the absence of water, a one-electron wave appears at $E_{1/2} = 1.04$ V for the $Ru^{III}-OH_2^{3+}/Ru^{II}-OH_2^{2+}$ couple, which is followed by barely discernible waves at $E_{1/2} = 1.4$ V for the $Ru^{IV}=O^{2+}/Ru^{III}-OH_2^{3+}$ couple and $E_{1/2} = 1.8$ V for the $Ru^{V}=O^{3+}/Ru^{IV}=O^{2+}$ couple. The latter are more obvious in square-wave voltammograms (SWVs) (Figure S5). The inhibited electrochemical response of the $Ru^{IV}=O^{2+}/Ru^{III}-OH_2^{3+}$ couple is due to PCET and

10.1021/ja107347n

the requirement of both electron and proton transfer at the electrode.[6] With added water, the catalytic water oxidation occurs at the onset for the oxidation of Ru(IV) to Ru(V). Addition of water shifts the $Ru^{III}-OH_2^{3+}/Ru^{II}-OH_2^{2+}$ couple negatively through an outer-sphere solvation effect, with $E_{1/2}$ reaching 0.94 V with 8% added water. CVs under the conditions in Figure 1a are stable indefinitely with respect to multiple scans.

The catalytic peak current for water oxidation, i_{cat}, at 1.8 V varies linearly with $[H_2O]^{1/2}$ to the limit of miscibility, 0−8% (0−4.4 M) in added water (Figure 1b). It also varies linearly with $[Ru^{II}-OH_2^{2+}]$ (Figure S6). Similar results were obtained in 1:1 PC/EC mixtures containing 0−12% (0−6.6 M) water (Figure S7), with evidence for saturation at higher concentrations. These observations are consistent with a electrocatalytic mechanism for water oxidation involving rate-limiting O-atom transfer to H_2O (Scheme 1), the rate law in eq 1, and the current expression in eq 2:[7]

$$\text{rate} = k_{cat}[Ru^{V}{=}O^{3+}] = k_o[Ru^{V}{=}O^{3+}][H_2O] \qquad (1)$$

$$\begin{aligned} i_{cat} &= nFA[Ru](k_{cat}D_{Ru})^{1/2} \\ &= nFA[Ru](k_oD_{Ru}[H_2O])^{1/2} \end{aligned} \qquad (2)$$

where $n = 4$ is the electrochemical stoichiometry, F is the Faraday constant, A is the electrode surface area (in cm^2), [Ru] is the concentration of catalyst (in mol/L), and $D_{Ru} \approx 0.7 \times 10^{-6}$ cm^2/s is the diffusion coefficient for catalyst **1** as determined by scan rate dependent measurements and the Randles−Sevcik equation. The same catalytic currents and value of $E_{1/2}(Ru-OH_2^{3+/2+})$ were obtained in 6% H_2O/PC with and without 30 mM HNO_3 (Figure S8), showing that local pH effects associated with water oxidation ($2H_2O \rightarrow O_2 + 4H^+ + 4e^-$) play no role in the electrochemical response.

As expected for a solution couple, a linear relationship between the peak current (i_d) for the Ru(III/II) couple and the square root of the scan rate ($v^{1/2}$) exists for $v = 3-1000$ mV/s (Figure S9b). The catalytic peak current normalized to the square root of the scan rate ($i_{p,a}/v^{1/2}$) increases with decreasing scan rate at low scan rates (Figure S9a), consistent with a rate-limiting step prior to electron transfer to the electrode and the mechanism in Scheme 1 with rate-limiting O-atom transfer from $Ru^{V}{=}O^{3+}$ to H_2O.

From the scan-rate-dependent measurements, a k_o value of ∼0.3 M^{-1} s^{-1} was obtained from the slope of a plot of i_{cat}/i_d versus $v^{-1/2}$ (Figure S9c) on the basis of eq 3, which was derived by use of the Randles−Sevcik equation to eliminate the dependence on [Ru], A, and D_{Ru}:[7]

$$\begin{aligned} \frac{i_{cat}}{i_d} &= 2.242\left(\frac{k_{cat}RT}{nFv}\right)^{1/2} \\ &= 2.242\left(\frac{k_oRT[H_2O]}{nFv}\right)^{1/2} \end{aligned} \qquad (3)$$

where T is the temperature (in K) and R is the gas constant. On the basis of this value of k_o, there is a rate enhancement of ∼300 for water oxidation by $Ru^{V}{=}O^{3+}$ in 6% (3.3 M) H_2O/PC ($k_{cat} \approx 1$ s^{-1}) relative to the same catalyst at pH 1 in aqueous solution ($k_{cat} \approx 3.1 \times 10^{-3}$ s^{-1}).[2b]

In water, the key O−O bond-forming step involves O-atom attack on H_2O by $Ru^{V}{=}O^{3+}$ in concert with proton transfer to a second water molecule or added base in a concerted atom−proton transfer (APT) pathway (eq 4):[8]

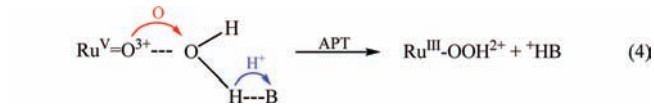

(4)

A significant H_2O/D_2O kinetic isotope effect (KIE) of up to ∼6.6 was observed for H_2O as the base.[8] In contrast, the rate law for the reaction in PC points to the involvement of a single water molecule and O-atom transfer to H_2O in the O−O bond-forming step. As shown by CV comparisons for **1** (Figure S10), $k_{cat,H_2O}/k_{cat,D_2O} = (i_{cat,H_2O}/i_{cat,D_2O})^2 \leq 1.4$ in PC. These observations are consistent with a different mechanism in PC, one involving a single water molecule and, presumably, direct O-atom transfer to give a coordinated hydrogen peroxide intermediate (eq 5):

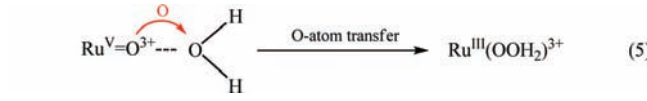

(5)

On the basis of initial density functional theory gas-phase calculations, the isomer $Ru^{III}(OOH_2)^{3+}$ is favored over $Ru^{III}(HOOH)^{3+}$ by ∼8 kcal/mol.[9] The nonaqueous rate enhancements and change in mechanism may be due to a higher activity for water and decreased acidity for $Ru^{III}(OOH_2)^{3+}$ in the largely organic solvent environment.[10]

As shown by the data in Figure 2 and Figure S11, there is also evidence for a competing APT pathway with added acetate ion, CH_3COO^- (OAc^-), in 1:1 mol/mol LiOAc/HOAc, with OAc^- as the proton-acceptor base and TFE as the solvent.[11] These experiments were conducted with 0.1 M $LiClO_4$ as the supporting electrolyte because $^nBu_4N^+$ is susceptible to oxidation under these conditions with added bases.

The data in Figure 2 and Figure S11 indicate the following:

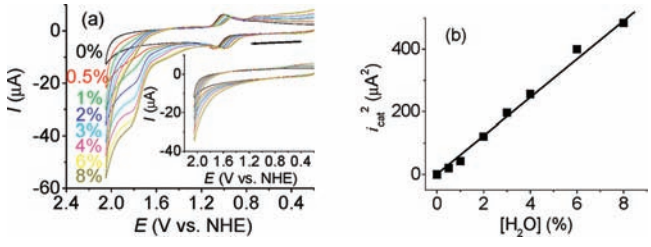

Figure 1. (a) CVs of 1 mM **1** in 0.1 M $^nBu_4NPF_6$/PC upon addition of increasing amounts of water, as indicated by the percentages in the figure. The inset shows the corresponding backgrounds in the absence of **1**. (b) Plot of i_{cat}^2 (background subtracted) at 1.85 V (vs NHE) vs $[H_2O]$ (see eq 2). Electrode, GC; scan rate, 100 mV/s.

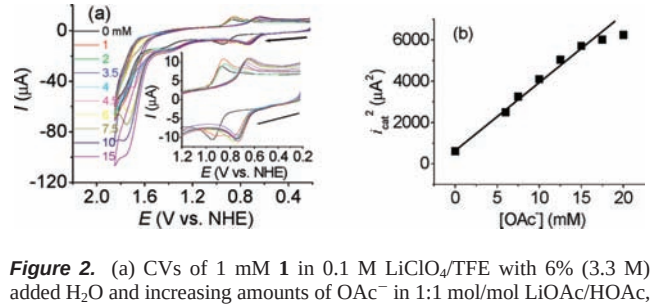

Figure 2. (a) CVs of 1 mM **1** in 0.1 M $LiClO_4$/TFE with 6% (3.3 M) added H_2O and increasing amounts of OAc^- in 1:1 mol/mol LiOAc/HOAc, as indicated by the concentrations in the figure. The inset shows a magnified view of the Ru(III/II) couple. (b) Plot of i_{cat}^2 (background subtracted) vs $[OAc^-]$. Catalytic currents for $[OAc^-] < 6$ mM were omitted because separate waves for direct and APT oxidation were observed (see the text). Electrode, GC; scan rate, 100 mV/s. Also see Figure S11.

(1) With no added OAc^-, the CV of **1** in 6% (v/v) H_2O/TFE is similar to that in H_2O/PC, with $E_{1/2}(Ru^{III}-OH_2^{3+}/Ru^{II}-OH_2^{2+}) = 0.92$ V, $E_{1/2}(Ru^{IV}=O^{2+}/Ru^{III}-OH_2^{3+}) = 1.38$ V, and $E_{p,a} = 1.8$ V for catalytic water oxidation. The diffusion coefficient increases to $D_{Ru} \approx 1.3 \times 10^{-6}$ cm^2/s, and the rate constant for water oxidation increases slightly to $k_o \approx 0.35$ M^{-1} s^{-1} with a KIE of ≤ 1.3.

(2) Upon addition of 1 mM OAc^-, a second Ru(III/II) wave appears at $E_{1/2} = 0.75$ V. It shifts slightly to $E_{1/2} = 0.70$ V at 3.5 mM OAc^-. There is no further shift at higher concentrations of added OAc^-, but this couple dominates as OAc^- is further increased. The shift to lower potential with added OAc^- is consistent with the appearance of the pH-dependent $Ru^{III}-OH^{2+}/Ru^{II}-OH_2^{2+}$ couple and its reported $E^{o\prime}$−pH diagram.[3]

(3) At 3.5−4.5 mM OAc^-, two separate water oxidation waves appear, with a new wave appearing at 1.7 V that points to the appearance of an APT pathway with added OAc^- as the proton-acceptor base. The waves merge past $[OAc^-] = 6$ mM, and the currents level off at $[OAc^-] \geq 15$ mM. As shown by the plot of i_{cat}^2 versus $[OAc^-]$ in the inset in Figure 2b, i_{cat}^2 increases linearly with $[OAc^-]$ from 6 to 15 mM. This observation is consistent with the rate law given by eqs 6:

$$\text{rate} = (k_o + k_B[OAc^-])[Ru^V{=}O^{3+}][H_2O] \quad (6a)$$

$$k_{cat} = (k_o + k_B[OAc^-])[H_2O] \quad (6b)$$

A k_B value of $\sim$260 M^{-2} s^{-1} was obtained from the scan-rate-dependent data in Figure S12 by use of eq 3. For comparison, $k_B \approx 10$ M^{-1} s^{-1} in water with OAc^- as the added base.[8]

The appearance of a new wave for the $Ru-OH_2^{3+/2+}$ couple with added OAc^- is consistent with formation of an ion pair between **1** and OAc^- and oxidation of the ion pair at 0.70 V. At even higher concentrations of added $[OAc^-]$, there is clear evidence for saturation kinetics, the ion-pair mechanism shown in eqs 7, and the rate law given by eqs 8, including a dependence on water concentration (Figure S13).[12] From a plot of $[(i_{cat,B}/i_{cat,o})^2 - 1]^{-1}$ versus $1/[OAc^-]$ at fixed $[H_2O]$ (Figure S14), the values $k_{APT} = 12 \pm 2$ M^{-1} s^{-1} and $K_{IP} = 19 \pm 3$ M^{-1} were obtained.

$$Ru^V{=}O^{3+} + OAc^- \overset{K_{IP}}{\rightleftharpoons} Ru^V{=}O^{3+}, OAc^- \quad (7a)$$

$$Ru^V{=}O^{3+}, OAc^- + H_2O \xrightarrow{k_{APT}} Ru^{III} - OOH^{2+} + HOAc \quad (7b)$$

$$Ru^{III}-OOH^{2+} + H_2O \rightarrow Ru^V{=}O^{3+} + O_2 + 3H^+ + 4e^- \quad (7c)$$

$$\text{rate} = \left(\frac{k_o + k_{APT}K_{IP}[OAc]}{1 + K_{IP}[OAc^-]}\right)[Ru^V{=}O^{3+}][H_2O] \quad (8a)$$

$$\frac{k_{cat}}{[H_2O]} = \frac{k_o + k_{APT}K_{IP}[OAc]}{1 + K_{IP}[OAc^-]} \quad (8b)$$

$$\left(\frac{k_{cat}}{k_o[H_2O]} - 1\right)^{-1} = \left[\left(\frac{i_{cat,B}}{i_{cat,o}}\right)^2 - 1\right]^{-1} = \frac{k_o}{k_{APT}} + \frac{k_o}{k_{APT}K_{IP}}\left(\frac{1}{[OAc^-]}\right) \quad (8c)$$

In Figure 3a is shown a CV of FTO|**1-PO$_3$H$_2$** in 0.1 M $LiClO_4$/PC with 6% H_2O, 30 mM in HNO_3, at 100 mV/s. The pattern of surface waves in PC is similar to those observed for the solution analogue with $E^{o\prime} = 0.89$ V for the $Ru^{III}-OH_2^{3+}/Ru^{II}-OH_2^{2+}$ couple, but there is additional mechanistic information. New waves appear at $E_{1/2} = 0.50$ and 0.35 V following an oxidative excursion to the water oxidation wave at 1.85 V. We tentatively assign these waves to the peroxidic couples $Ru^{IV}(OO)^{2+}/Ru^{III}(OOH_2)^{3+}$ and $Ru^{III}(OOH_2)^{3+}/Ru^{II}(OOH_2)^{2+}$. CV evidence for peroxidic couples in water has been reported previously.[3] The appearance of the peroxidic waves indicates that under these conditions, further oxidation of $Ru^{IV}(OO)^{2+}$ and O_2 loss are in competition with reduction of the intermediate on the electrode surface (see Scheme 1).

As shown by the data in Figure 3b, the APT pathway also appears for surface electrocatalytic water oxidation in 0.1 M $LiClO_4$/TFE with 6% H_2O and added OAc^-. The shift in the $E_{1/2}$ values for the Ru(III/II) couple in going from added HNO_3 to OAc^- is consistent with the pH dependence of the Ru(III/II) couple as noted above.

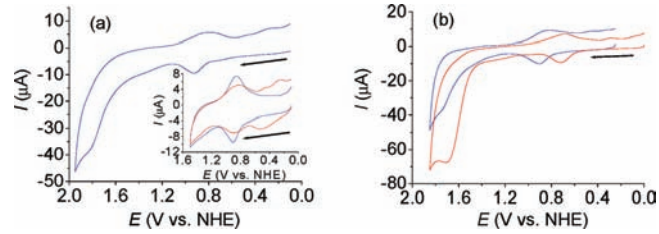

Figure 3. (a) CV of FTO|**1-PO$_3$H$_2$** in 0.1 M $LiClO_4$/PC with 6% (3.3 M) H_2O, 30 mM in HNO_3. The inset shows CVs of FTO|**1-PO$_3$H$_2$** before (blue line) and after (red line) a potential scan through the catalytic oxidation wave at 1.85 V. (b) CVs of FTO|**1-PO$_3$H$_2$** in 0.1 M $LiClO_4$/TFE with 6% (3.3 M) H_2O, with 30 mM HNO_3 (blue line) or 15 mM in OAc^- in 1:1 mol/mol LiOAc/HOAc (red line). Scan rate, 100 mV/s.

Electrocatalytic water oxidation was investigated at ITO|*nano*ITO|**1-PO$_3$H$_2$** with 0.2 mM **1-PO$_3$H$_2$** in the external solution in 15% H_2O, 1:1 PC/EC mixtures at an applied potential of 1.85 V (vs NHE) (Figure S15). Steady-state catalytic current densities of 70 $\mu A/cm^2$ were obtained during the electrolysis over extended periods. Under these conditions, the surface mechanism is presumably that shown in Scheme 1 but with $Ru^{III}(OOH_2)^{3+}$ as an intermediate rather than $Ru^{III}-OOH^{2+}$. Further oxidation of $Ru^{III}(OOH_2)^{3+}$ with proton loss to give $Ru^{IV}(OO)^{2+}$ followed by the remainder of the cycle results in oxygen evolution. In the electrocatalytic experiments, released protons (as H_3O^+) in the 15% H_2O, 1:1 PC/EC mixture are reduced at the auxiliary electrode ($2H^+ + 2e^- \rightarrow H_2$). After 12 h of electrolysis at 1.85 V, $\sim$12.0 μmol of O_2 was detected by an oxygen electrode (Ocean Optics NeoFox, HIOXY), corresponding to $\sim$400 turnovers and a Faradaic efficiency of 70%. Electrolysis at ITO|*nano*ITO|**1-PO$_3$H$_2$** with 0.2 mM **1-PO$_3$H$_2$** in 0.1 M $LiClO_4$/TFE with 15% H_2O and 15 mM OAc^- at 1.75 V occurred with a catalytic current density of 120 $\mu A/cm^{-2}$ and a Faradaic efficiency of 65% over an electrolysis period of 12 h.

The results of this study are significant in demonstrating not only that catalytic water oxidation can occur in nonaqueous environments but also that it occurs with greatly enhanced rates and by a new pathway involving direct O-atom addition to H_2O. There may be important implications in these results for alternate solar-fuel strategies in nonaqueous environments.

Acknowledgment. Funding by the Army Research Office through Grant W911NF-09-1-0426 supporting Z.C.; the UNC Energy Frontier Research Center (EFRC) Solar Fuels and Next Generation Photovoltaics, an EFRC funded by the U.S. Department of Energy, Office of Science, Office of Basic Energy Sciences,

under Award DE-SC0001011 supporting J.J.C. and H.L.; and the Center for Catalytic Hydrocarbon Functionalization, an EFRC funded by the U.S. Department of Energy, Office of Science, Office of Basic Energy Sciences under Award DE-SC0001298 supporting J.F.H. and A.P. is gratefully acknowledged.

Supporting Information Available: Additional information as noted in the text. This material is available free of charge via the Internet at http://pubs.acs.org.

References

(1) (a) McDaniel, N. D.; Coughlin, F. J.; Tinker, L. L.; Bernhard, S. *J. Am. Chem. Soc.* **2008**, *130*, 210. (b) Tseng, H.-W.; Zong, R.; Muckerman, J. T.; Thummel, R. *Inorg. Chem.* **2008**, *47*, 11763. (c) Hull, J. F.; Balcells, D.; Blakemore, J. D.; Incarvito, C. D.; Eisenstein, O.; Brudvig, G. W.; Crabtree, R. H. *J. Am. Chem. Soc.* **2009**, *131*, 8730. (d) Masaoka, S.; Sakai, K. *Chem. Lett.* **2009**, *38*, 182. (e) Wasylenko, D. J.; Ganesamoorthy, C.; Koivisto, B. D.; Henderson, M. A.; Berlinguette, C. P. *Inorg. Chem.* **2010**, *49*, 2202. (f) Gao, Y.; Åkermark, T.; Liu, J. H.; Sun, L. C.; Åkermark, B. *J. Am. Chem. Soc.* **2009**, *131*, 8726. (g) Duan, L. L.; Xu, Y. H.; Zhang, P.; Wang, M.; Sun, L. C. *Inorg. Chem.* **2010**, *49*, 209. (h) Romain, S.; Vigara, L.; Llobet, A. *Acc. Chem. Res.* **2009**, *42*, 1944.

(2) (a) Concepcion, J. J.; Jurss, J. W.; Templeton, J. L.; Meyer, T. J. *J. Am. Chem. Soc.* **2008**, *130*, 16462. (b) Concepcion, J. J.; Tsai, M.-K.; Muckerman, J. T.; Meyer, T. J. *J. Am. Chem. Soc.* **2010**, *132*, 1545. (c) Concepcion, J. J.; Jurss, J. W.; Norris, M. R.; Chen, Z. F.; Templeton, J. L.; Meyer, T. J. *Inorg. Chem.* **2010**, *49*, 1277. (d) Concepcion, J. J.; Jurss, J. W.; Brennaman, M. K.; Hoertz, P. G.; Patrocinio, A. O. T.; Iha, N. Y. M.; Templeton, J. L.; Meyer, T. J. *Acc. Chem. Res.* **2009**, *42*, 1954.

(3) (a) Chen, Z. F.; Concepcion, J. J.; Jurss, J. W.; Meyer, T. J. *J. Am. Chem. Soc.* **2009**, *131*, 15580. (b) Chen, Z. F.; Concepcion, J. J.; Hull, J. F.; Hoertz, P. G.; Meyer, T. J. *Dalton Trans.* **2010**, *39*, 6950.

(4) (a) Barber, J. *Biochem. Soc. Trans.* **2006**, *34*, 619. (b) Renger, G.; Renger, T. *Photosynth. Res.* **2008**, *98*, 53. (c) Holzwarth, A. R.; Mueller, M. G.; Reus, M.; Nowaczyk, M.; Sander, J.; Roegner, M. *Proc. Natl. Acad. Sci. U.S.A.* **2006**, *103*, 6895. (d) Meyer, T. J.; Huynh, M. H. V.; Thorp, H. H. *Angew. Chem., Int. Ed.* **2007**, *46*, 5284.

(5) Hoertz, P. G.; Chen, Z. F.; Kent, C. A.; Meyer, T. J. *Inorg. Chem.* **2010**, *49*, 8179.

(6) Trammell, S. A.; Wimbish, J. C.; Odobel, F.; Gallagher, L. A.; Narula, P. M.; Meyer, T. J. *J. Am. Chem. Soc.* **1998**, *120*, 13248.

(7) (a) Bard, A. J.; Faulkner, L. R. *Electrochemical Methods: Fundamentals and Applications*, 2nd ed.; Wiley: New York, 2001. (b) Zanello, P. *Inorganic Electrochemistry: Theory, Practice and Application*; Royal Society of Chemistry: Cambridge, U.K., 2003. (c) Kutner, W.; Meyer, T. J.; Murray, R. W. *J. Electroanal. Chem.* **1985**, *195*, 375.

(8) Chen, Z. F.; Concepcion, J. J.; Hu, X. Q.; Yang, W. T.; Hoertz, P. G.; Meyer, T. J. *Proc. Natl. Acad. Sci. U.S.A.* **2010**, *107*, 7225.

(9) Lin, X. S.; Hu, X. Q.; Yang, W. T. Unpublished results.

(10) (a) Muzikar, J.; van de Goor, T.; Gaš, B.; Kenndler, E. *Anal. Chem.* **2002**, *74*, 428. (b) Cantu, M. D.; Hillebrand, S.; Carrilho, E. *J. Chromatogr., A* **2005**, *1068*, 99.

(11) The selection of appropriate bases in nonaqueous solvents is limited by solubility and oxidative stability: (1) Lithium acetate (CH_3CO_2Li) is difficult to dissolve in PC. (2) Lithium phosphate (LiH_2PO_4, Li_2HPO_4, or Li_3PO_4) is not soluble in PC or TFE. (3) Organic bases such as phthalate, histidine, citrate, or 4-(2-hydroxyethyl)-1-piperazineethanesulfonate (HEPES) are oxidized at the electrode or by $Ru^{V}{=}O^{3+}/Ru^{IV}{=}O^{2+}$.

(12) There is evidence for a direct reaction between $Ru^{V}{=}O^{3+}$ and OAc^{-} with no added water; this is currently under investigation.

JA107347N